

**Climatology, seasonality and trends of oceanic coherent  
eddies**

**Josué Martínez-Moreno<sup>1</sup>, Andrew McC. Hogg<sup>1</sup>, and Matthew H. England<sup>2</sup>**

<sup>4</sup> Research School of Earth Science and ARC Center of Excellence for Climate Extremes, Australian  
<sup>5</sup> National University, Canberra, Australia

<sup>6</sup> Climate Change Research Centre (CCRC), UNSW Australia, Sydney NSW, Australia

**Key Points:**

- <sup>8</sup> Kinetic energy of coherent eddies contain around 50% of the surface ocean kinetic  
<sup>9</sup> energy budget.
- <sup>10</sup> Seasonal cycle of the number of coherent eddies and coherent eddy amplitude re-  
<sup>11</sup> veal a 3-6 month lag to wind forcing
- <sup>12</sup> Seasonal lag between the number of coherent eddies and eddy amplitude.
- <sup>13</sup> The coherent eddy amplitude has increase at a rate of 3 cm per decade since 1993.

14      **Abstract**

15      Ocean eddies influence regional and global climate through mixing and transport  
 16      of heat and properties. One of the most recognizable and ubiquitous feature of oceanic  
 17      eddies are vortices with spatial scales of tens to hundreds of kilometers, frequently re-  
 18      ferred as “mesoscale eddies” or “coherent eddies”. Coherent eddies are known to trans-  
 19      port properties across the ocean and to locally affect near-surface wind, cloud proper-  
 20      ties and rainfall patterns. Although coherent eddies are ubiquitous, yet their climatol-  
 21      ogy, seasonality and long-term temporal evolution remains poorly understood. Thus, we  
 22      examine the kinetic energy contained by coherent eddies and we present the annual, in-  
 23      terannual, and long-term changes of automatically identified coherent eddies from satel-  
 24      lite observations from 1993 to 2018. Around 50% of the kinetic energy contained by ocean  
 25      eddies corresponds to coherent eddies. Additionally, a strong hemispherical seasonal cy-  
 26      cle is observed, with a 3–6 months lag between the wind forcing and the response of the  
 27      coherent eddy field. Furthermore, the seasonality of the number of coherent eddies and  
 28      their amplitude reveals that the number of coherent eddies responds faster to the forc-  
 29      ing (~3 months), then the coherent eddy amplitude (which is lagged by ~6 months). Our  
 30      analysis highlights the relative importance of the coherent eddy field in the ocean ki-  
 31      netic energy budget, implies a strong response of the eddy number and eddy amplitude  
 32      to forcing at different time-scales, and showcases the seasonality, and multidecadal trends  
 33      of coherent eddy properties.

34      **Plain language summary**

35      **1 Introduction**

36      Mesoscale ocean variability with spatial scales of tens to hundreds of kilometers is  
 37      comprised of processes such as vortices, waves, and jets (Ferrari & Wunsch, 2009; Fu et  
 38      al., 2010). These mesoscale processes are highly energetic, and they play a crucial role  
 39      in the transport of heat, salt, momentum, and other tracers through the ocean (Wun-  
 40      sch & Ferrari, 2004; Wyrtki et al., 1976; Gill et al., 1974). Possibly, the most recogniz-  
 41      able and abundant process observed from satellites is mesoscale vortices. Although mesoscale  
 42      vortices are commonly referred to in literature as “mesoscale eddies”, this term is also  
 43      often used to describe the total mesoscale ocean variability (the time-varying component  
 44      of the mesoscale flow), thus, here we will refer to mesoscale vortices as *coherent eddies*.

45 Coherent eddies are quasi-circular currents. According to their rotational direction,  
46 the sea surface height anomaly within a coherent eddy can have a negative or positive  
47 sea surface height anomaly (cold-core and warm-core coherent eddies, respectively). This  
48 characteristic sea surface height signature of coherent eddies has been utilized to auto-  
49 matically identify and track coherent eddies from satellite altimetry (Cui et al., 2020;  
50 Martínez-Moreno et al., 2019; Ashkezari et al., 2016; Faghmous et al., 2015; Chelton et  
51 al., 2007). Automated identification algorithms of coherent eddies have shown their ubiq-  
52 uituity in the oceans, with a predominant influence at hotspots of eddy activity such as bound-  
53 ary currents and the Antarctic Circumpolar Current. In these regions, Chelton et al. (2011)  
54 estimated that coherent eddies contribute around 40–50% of the mesoscale kinetic en-  
55 ergy (Chelton et al., 2011) and thus a significant fraction of the total kinetic energy (Fer-  
56 rari & Wunsch, 2009). Although this unique estimate showcases the importance of the  
57 mesoscale coherent eddy field, the energy contained by coherent eddies was estimated  
58 by extracting the geostrophic velocities within the detected coherent eddies, thus it is  
59 possible it may contain energy from other processes. Coherent eddies are not only abun-  
60 dant and may have a large proportion of the surface kinetic energy budget, but they are  
61 also essential to ocean dynamics as concluded by many previous studies (Patel et al., 2020;  
62 Schubert et al., 2019; Pilo et al., 2015; Frenger et al., 2015, 2013; Beron-Vera et al., 2013;  
63 Siegel et al., 2011; Hogg & Blundell, 2006).

64 There is broad consensus that mesoscale eddy kinetic energy has a pronounced sea-  
65 sonal variability (Uchida et al., 2017; Kang & Curchitser, 2017; Qiu & Chen, 2004; Qiu,  
66 1999). Several hypotheses have been proposed to explain this seasonality including: sea-  
67 sonal variations of atmospheric forcing (Sasaki et al., 2014), seasonality of the mixed layer  
68 depth (Qiu et al., 2014; Callies et al., 2015), seasonality of the intensity of barotropic in-  
69 stability (Qiu & Chen, 2004), the variability of the baroclinic instability due to the sea-  
70 sonality of the vertical shear (Qiu, 1999), and a seasonal lag of the inverse energy cas-  
71 cade (energy is transported between scales from small to large; Arbic et al., 2013) in com-  
72 bination with the presence of a front in the mixed layer, which can lead to a seasonal  
73 cycle of the baroclinic instability (Qiu et al., 2014). On one hand, processes such as barotropic  
74 and baroclinic instabilities control the seasonality of coherent eddies in the ocean. On  
75 the other hand, recent studies using observations and eddy-permitting climate models  
76 suggest several long-term adjustments of the global ocean capable of long-term changes  
77 in the coherent eddy field. Such readjustments include a multidecadal increase in the ocean

stratification resulted from temperature and salinity changes (Li et al., 2020), a horizontal readjustment of the sea surface temperature gradients (Ruela et al., 2020; Bouali et al., 2017; Cane et al., 1997), and an intensification of the kinetic energy, eddy kinetic energy, and mesoscale eddy kinetic energy over the last 3 decades as a consequence of an increase in wind forcing (Hu et al., 2020; Wunsch, 2020; Martínez-Moreno et al., 2021). All these seasonal factors and long-term readjustments directly influence the annual and decadal response of the coherent eddy field, however, the seasonality of the coherent component of the eddy kinetic energy, as well as the seasonal cycle and trends of the coherent eddy statistics remain unknown.

Here we present a new global climatology of the coherent eddy kinetic energy by reconstructing the coherent eddy signature from satellite observations. Our climatology documents the seasonal cycle of the coherent eddy kinetic energy, and seasonal cycle and long-term trends of the coherent eddy properties over the satellite record. Moreover, we conduct more detail analysis in regions where coherent eddies dominate the eddy kinetic energy field. This paper is structured as follows: the data sources and methodology are described in section 2. Then, we present the climatology, energy ratios, and global seasonality of the coherent eddy kinetic energy in subsection 3. Subsection 4 presents the global climatology and seasonality of coherent eddy properties, followed by the seasonal cycle and coherent eddy property time-series in regions dominated by coherent eddies (subsection 6.1). We then focus our attention on the long-term changes of the coherent eddy properties (section 5). Finally, section 7 summarizes the main results and discusses the implications of this study.

## 2 Methods

We use daily sea surface height (SSH) data made available by the Copernicus Marine Environment Monitoring Service in near real time (CMEMS, 2017). This gridded product contains the sea surface height and geostrophic velocities with daily  $0.25^\circ$  resolution from January 1993 to 2019. The daily geostrophic velocities allowed us to compute the kinetic energy (KE) and eddy kinetic energy (EKE) over the satellite record. The main source of EKE is the time-varying wind (Ferrari & Wunsch, 2009), thus we computed the seasonal cycle of the wind magnitude from the JRA55 reanalysis (Japan Meteorological Agency, Japan, 2013) using wind velocities at 10m above the ocean's surface.

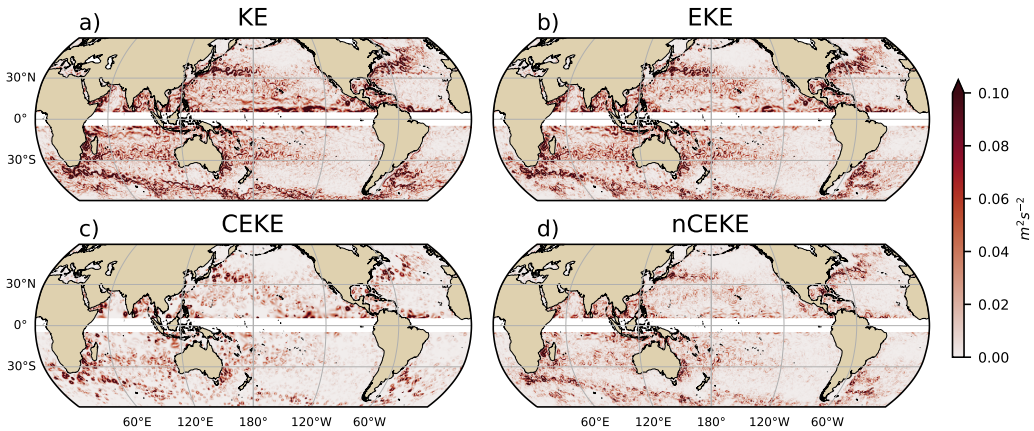
Over the same record, coherent eddy statistics from Martínez-Moreno et al. (2019), hereafter M-M, are analyzed and compared to those released by Chelton & Schlax (2013), both datasets are gridded in a  $1^\circ$  resolution. Although both datasets are produced via automated eddy identification algorithms using closed contours of SSH, these datasets have important differences in the criteria they use to identify and record coherent eddies statistics. The major difference include; (i) M-M's algorithm requires an adjustment between a 2D Gaussian and the SSH anomaly (SSHa) surface within the identify closed contour, while Chelton's only uses the outer-most closed contour of SSH; (ii) M-M's dataset reports the maximum SSHa within the identified coherent eddy, while Chelton's algorithm reports the maximum SSH value minus the discrete level in which the coherent eddy was identified; M-M's dataset includes all detected coherent eddies, while Chelton's dataset excludes (iii) coherent eddies with lifetimes shorter than four weeks and (iv) coherent eddy amplitudes smaller than 1cm. Moreover, M-M's algorithm allows the reconstruction of the coherent eddy field under the assumption that coherent eddies have a 2D Gaussian imprint in the sea surface height. These Gaussian anomalies then allow us to estimate the coherent geostrophic eddy velocities and thus the kinetic energy contained only by coherent eddies.

## 2.1 Kinetic Energy decomposition

Kinetic energy is commonly divided into the mean and time-varying components through a Reynolds decomposition. At a given time, the velocity field  $\mathbf{u} = (u, v)$  is split into the time mean ( $\bar{\mathbf{u}}$ ) and time varying components ( $\mathbf{u}'$ ). Moreover, M-M proposed to further decompose the eddy kinetic energy into the energy contained by coherent features ( $\mathbf{u}'_e$ ) and non-coherent features ( $\mathbf{u}'_n$ ). Therefore the KE equation can be written as:

$$\text{KE} = \underbrace{\bar{u}^2 + \bar{v}^2}_{\text{MKE}} + \underbrace{u'^2_e + v'^2_e + u'^2_n + v'^2_n}_{\text{CEKE}} + \underbrace{\mathcal{O}_c^2 + \mathcal{O}^2}_{\text{nCEKE}} \quad (1)$$

Due to the properties of this decomposition, the second order term  $\mathcal{O}^2$  is zero when averaged over the same period as  $\bar{\mathbf{u}}$ . However,  $\mathcal{O}_c^2$  is negligible when averaged over time and space. More information about the decomposition of the field into coherent features and non-coherent features is explained by Martínez-Moreno et al. (2019). A global snap-



143 **Figure 1.** Snapshot of surface kinetic energy ( $\overline{KE}$ ), surface eddy kinetic energy ( $\overline{EKE}$ ),  
 144 surface coherent eddy kinetic energy ( $\overline{CEKE}$ ), and surface non-coherent eddy kinetic energy  
 145 ( $\overline{nCEKE}$ ) for the 1st of January 2017.

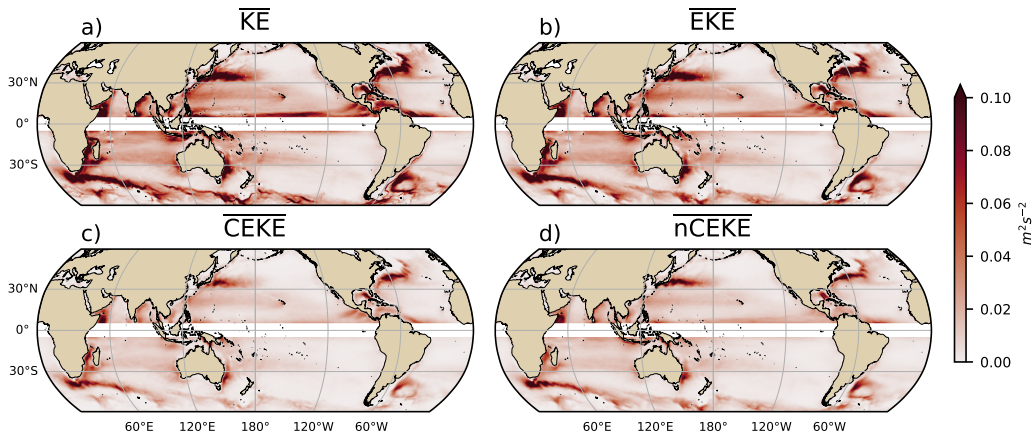
138 shot of each component of kinetic energy decomposition is shown in figure 1, where the  
 139 KE and EKE are comprised of rings and filaments. As expected, the decomposition of  
 140 EKE into CEKE and nCEKE components exhibit only ring-like signatures expected of  
 141 coherent eddies, while the non-coherent component shows filaments and some uniden-  
 142 tified coherent eddies.

## 146 2.2 Eddy statistics

147 The eddy statistics used in this study include the eddy count ( $cEddy_n$ ) defined as  
 148 the number of eddies per grid cell, and the mean eddy amplitude defined as the mean  
 149 amplitude of the coherent eddies within the cell ( $cEddy_{amp}$ ). The latter metric can be  
 150 separated into positive ( $cEddy_{amp}^+$ ) and negative ( $cEddy_{amp}^-$ ) coherent eddy amplitudes,  
 151 defined as the mean amplitude of warm core and cold core coherent eddies, respectively,  
 152 within the cell. The absolute eddy amplitude ( $|cEddy_{amp}|$ ) is then defined as:

$$|cEddy_{amp}| = \frac{1}{2} (cEddy_{amp}^+ - cEddy_{amp}^-) \quad (2)$$

153 Note that the  $cEddy_{amp}^+$  and  $cEddy_{amp}^-$  are sign definite, thus the difference will always  
 154 be positive, mean  $cEddy_{amp}$  can be negative or positive noting the dominant polarity  
 155 of coherent eddies in the region. We analyze the climatology, seasonal cycles and trends  
 156 of the eddy statistics between 1993 and 2019. We exclude the equatorial region ( $10^\circ S$   
 157 -  $10^\circ N$ ) and poleward of  $60^\circ$ . Note that the climatology of  $cEddy_n$  is computed by adding



173 **Figure 2.** Climatology of surface kinetic energy ( $\overline{KE}$ ), surface eddy kinetic energy ( $\overline{EKE}$ ),  
174 surface coherent eddy kinetic energy ( $\overline{CEKE}$ ), and surface non-coherent eddy kinetic energy  
175 ( $\overline{nCEKE}$ ) between 1993-2018.

158 all the identified eddies over the record, while all other climatological statistics are com-  
159 puted as the time-average over the record. Seasonal climatologies are calculated for the  
160 monthly average of each coherent eddy statistic, while hemispherical time-series are fil-  
161 tered with a running average of 90 days. Trends of  $cEddy_n$  and  $|cEddy_{amp}|$  are calcu-  
162 lated by coarsening the dataset to a  $5^\circ$  grid, and then linear trends are computed for each  
163 grid point, the statistical significance is assessed by a modified Mann-Kendall test (Yue  
164 & Wang, 2004). Time averages are denoted by  $\overline{\quad}$ , while spatial averages are shown  
165 by  $\langle \quad \rangle$ .

### 166 3 Global Coherent Eddy Energetics

#### 167 **Figure 2**

- 168 • All KE components have large energy contents in the boundary currents and antarc-  
169 tic circumpolar current.
- 170 • In many cases is the same, but there actually some differences There are several  
171 regions where the coherent component is larger than the non-coherent, we will in-  
172 vestigate these in more detail in section XX.

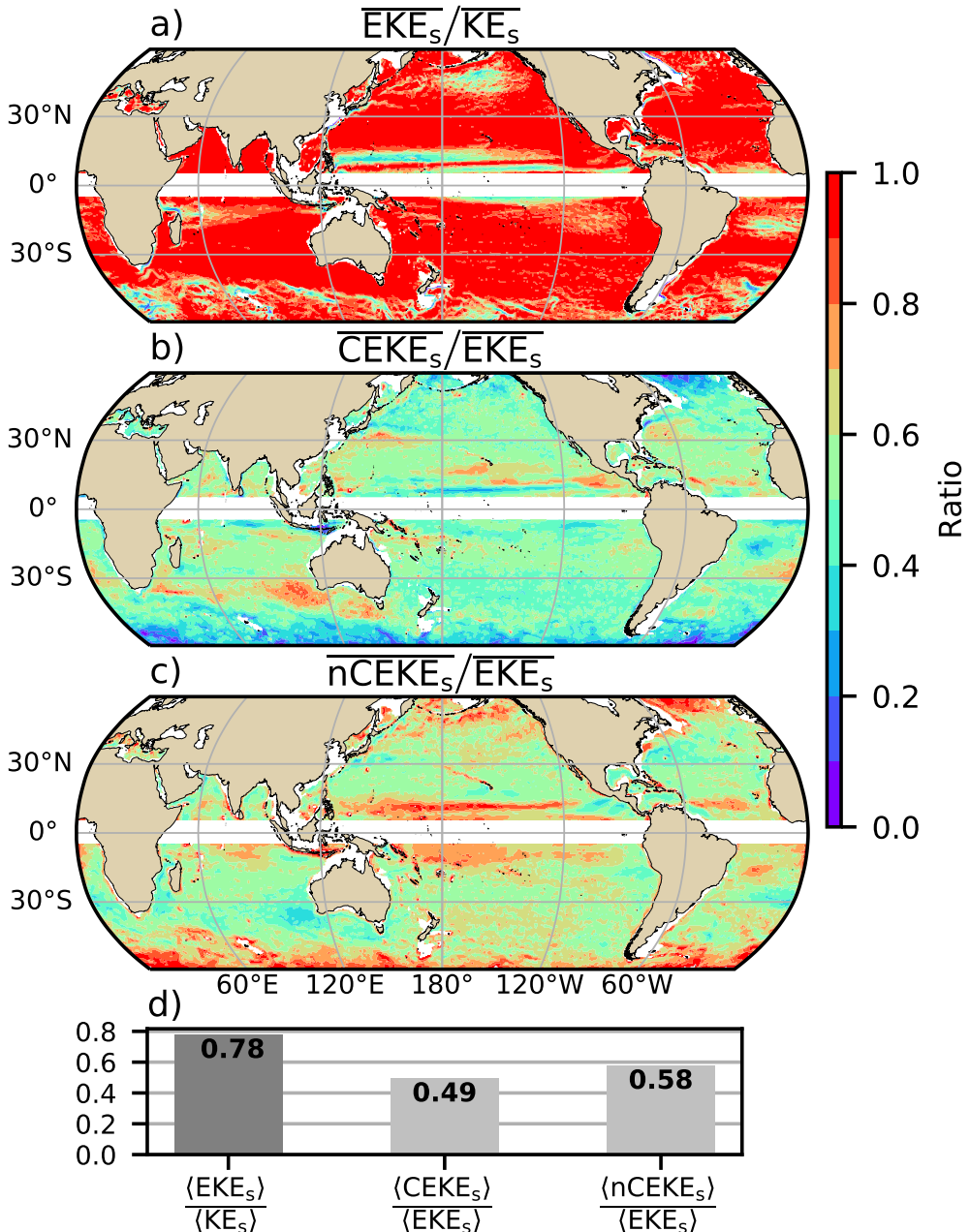
#### 176 **Figure 3**

- $\overline{\text{EKE}}$  is responsible of almost all the  $\overline{\text{KE}}$  across the ocean, except for regions with persistent currents over time, such as the mean boundary current locations, equatorial pacific currents and regions in the Antarctic Circumpolar current, where the EKE explains around 40% of the  $\overline{\text{KE}}$
- This estimate is consistent with that of Chelton.
- EKE Explains 80% of  $\overline{\text{KE}}$ , while  $\overline{\text{CEKE}}$  is 45% of  $\overline{\text{EKE}}$  and  $\overline{\text{nCEKE}}$  is 60% of  $\overline{\text{EKE}}$
- $\overline{\text{CEKE}}$  is large equatorwards from the Kuroshio current and Agulhas current.
- Areas with the largest coherent contribution are located in the South of Australia  $\overline{\text{CEKE}}$  and South Atlantic
- 
- $\overline{\text{nCEKE}}$  has a large amount of energy at high latitudes, this could be a consequence of the satellites not resolving the mesoscale coherent eddies.
- Global averages of the ratios show  $\overline{\text{EKE}}$  explains around 78% of the ocean *MKE* field, while coherent eddies and non coherent eddy features contain 49% and 59% per decade. Note this values don't add to 1 as there are cross terms that contain around XX% of the total energy.

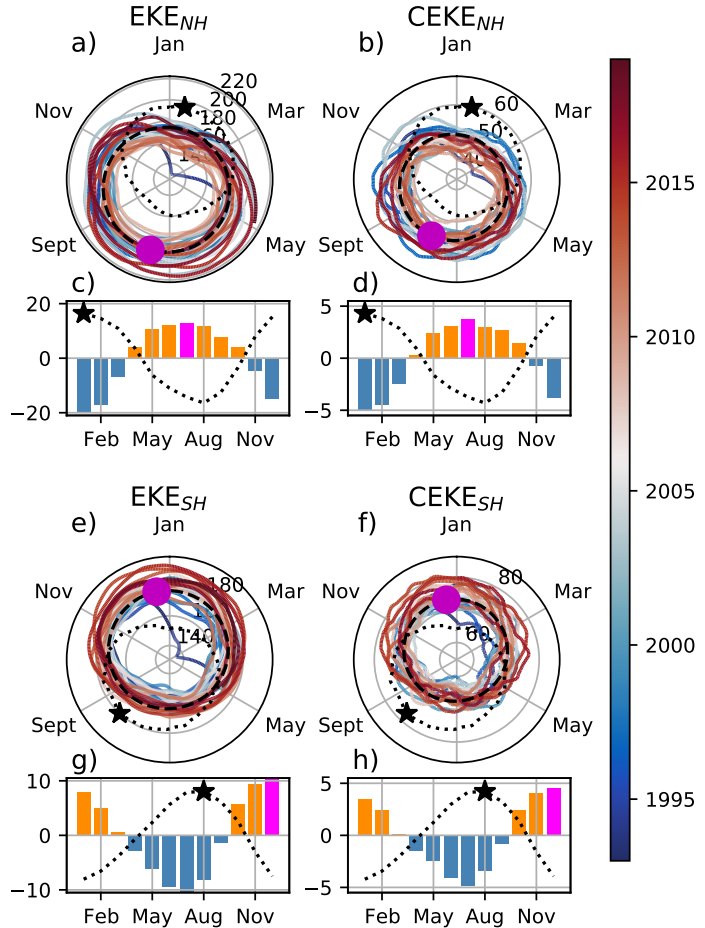
### 3.0.1 Seasonality

#### Figure 4

- The hemisphere seasonality show the EKE and CEKE peak in summer.
- Response of the EKE and CEKE show a seasonal lag of  $\sim$ 6 months to the forcing of the Winds. Make sure to note the maximum over the hemisphere, locally, the winds may peak in different months.
- Methods, explain more about winds or here.
- The coherent eddy field show a large interannual variability.
- In the Southern Ocean we observe a concentric growth as time passes, which support the increasing trends in the Southern Ocean observed by (Hogg et al., 2015; Martínez-Moreno et al., 2019; Martínez-Moreno et al., 2021)
- Point that in the northern hemisphere in winter the CEKE appears to be decreasing.



194 **Figure 3.** Ratios of the kinetic energy components. a) Map of the proportion of mean eddy  
 195 kinetic energy ( $EKE_s$ ) versus mean kinetic energy ( $\overline{KE}$ ); b) Map of the percentage of mean co-  
 196 herent eddy kinetic energy ( $\overline{CEKE}_s$ ) versus mean eddy kinetic energy ( $\overline{EKE}_s$ ); c) Map of the  
 197 percentage of mean non-coherent eddy kinetic energy ( $\overline{nCEKE}_s$ ) versus mean eddy kinetic energy  
 198 ( $\overline{EKE}_s$ ); d) Global averaged percentage of mean eddy kinetic energy ( $\langle \overline{EKE} \rangle$ ) versus the global  
 199 mean kinetic energy ( $\langle \overline{KE} \rangle$ ), and percentage of mean coherent eddy kinetic energy ( $\langle \overline{CEKE} \rangle$ )  
 200 and mean non coherent eddy kinetic energy ( $\langle \overline{nCEKE} \rangle$ ) versus global mean eddy kinetic energy  
 201 ( $\langle \overline{EKE} \rangle$ ).



215 **Figure 4.** Hemispherical seasonality of eddy kinetic energy (EKE), coherent eddy kinetic en-  
 216 ergy (CEKE). Panels a, and b show the northern hemisphere seasonal cycle, while panels c, and  
 217 d correspond to the southern hemisphere. Dashed lines correspond to the seasonal cycle of the  
 218 fields and dotted lines show the seasonal cycle of the wind magnitude smoothed over 120 days  
 219 (moving average). The green and magenta stars show the maximum of the seasonal cycle for the  
 220 kinetic energy components and the wind magnitude, respectively. The line colors show the year.

221      **4 Global Coherent Eddy Statistics**

222      **Figure 5**

- 223      • A comparison with previous identified numbers show a consistent pattern in the  
224      eddy count. The difference in the magnitude could be a consequence of Chelton  
225      et al. (2007) filtering the coherent eddies with lifespans longer than 16 weeks.
- 226      • Both datasets show a large number of eddies in the East North Pacific, East North  
227      Atlantic, as well as the East South Pacific, East South Atlantic and East Indian  
228      Ocean.
- 229      • While the number of eddies detected in the tropics is quite small.
- 230      • Furthermore, there are hotspots of numbers of eddies in other regions of the ocean,  
231      such as boundary currents and the Antarctic Circumpolar Current.
- 232      • An interesting feature shown in both datasets is a predominant patchiness where  
233      the count of the eddies is much larger. These puzzling pattern remains unknown.  
234      Although it looks like a propagation pattern, it could be that eddies persist for  
235      longer in those areas.
- 236      • The eddy amplitude as expected is maximum at the boundary currents and hotspots  
237      in the southern ocean.
- 238      • Interior of the gyres we can observe that there is an important amplitude of the  
239      coherent eddy field.
- 240      • Preferred eddy amplitude sign in boundary currents; positive amplitude polewards  
241      to the boundary current mean location, and negative amplitude equatorwards. This  
242      is consistent with the shed of coherent eddies from the boundary currents.
- 243      • There regions with large CEKE ratio show also a large coherent eddy amplitude.
- 244      • Absolute eddy amplitude has the similar signature as CEKE.

250      **4.0.1 Seasonality**

251      **Figure 6**

- 252      • Seasonality of the number of eddies in the Northern Hemisphere peaks on May,  
253      while the Southern Hemisphere peaks on October.
- 254      • The seasonality of the amplitude of the eddies is consistent with those of the Co-  
255      herent eddy kinetic energy.

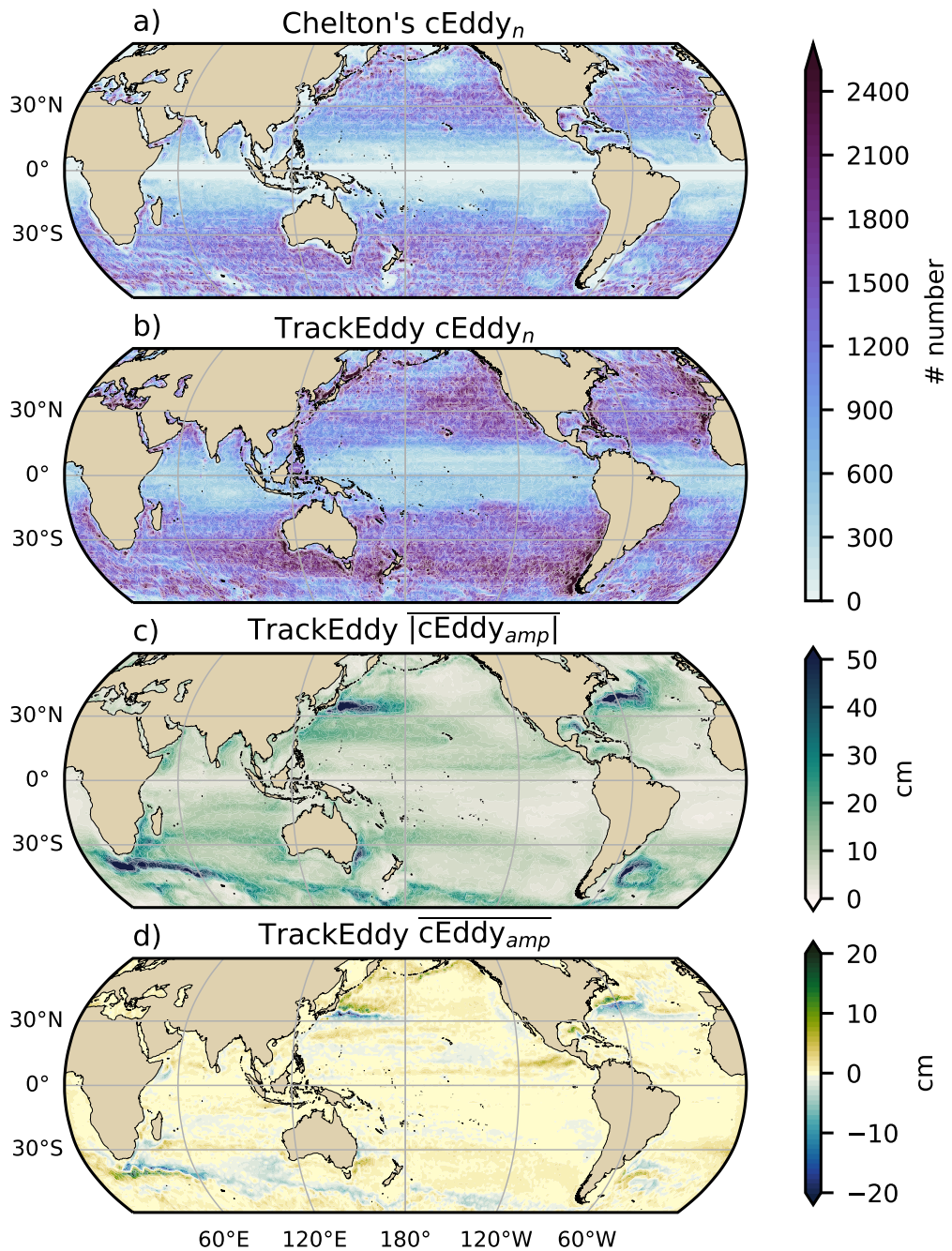


**Figure 5.** Climatology of the coherent eddy statistics. a) Climatology of the number of coherent eddies ( $cEddy_n$ ) identified by Chelton et al. (2007); b) Climatology of the number of coherent eddies ( $cEddy_n$ ) identified by Martínez-Moreno et al. (2019); c) Climatology of the mean absolute coherent eddy amplitude ( $cEddy_{amp}$ ). d) Climatology of the mean coherent eddy amplitude ( $cEddy_{amp}$ ).

- Interestingly, there is a 3 month lag to between the winds and the seasonality of the number of eddies, while the eddy amplitude responds approximately 6 months after the maximum winds.
- Note that both coherent eddy amplitudes seem to peak around the same time.
- If we look closely, the growing-shrinking concentric circles correspond to an increasing-decreasing trend. These are particularly obvious as a decrease in the eddy number in the Southern Hemisphere, and a increase in the eddy amplitude.

**Figure 6**

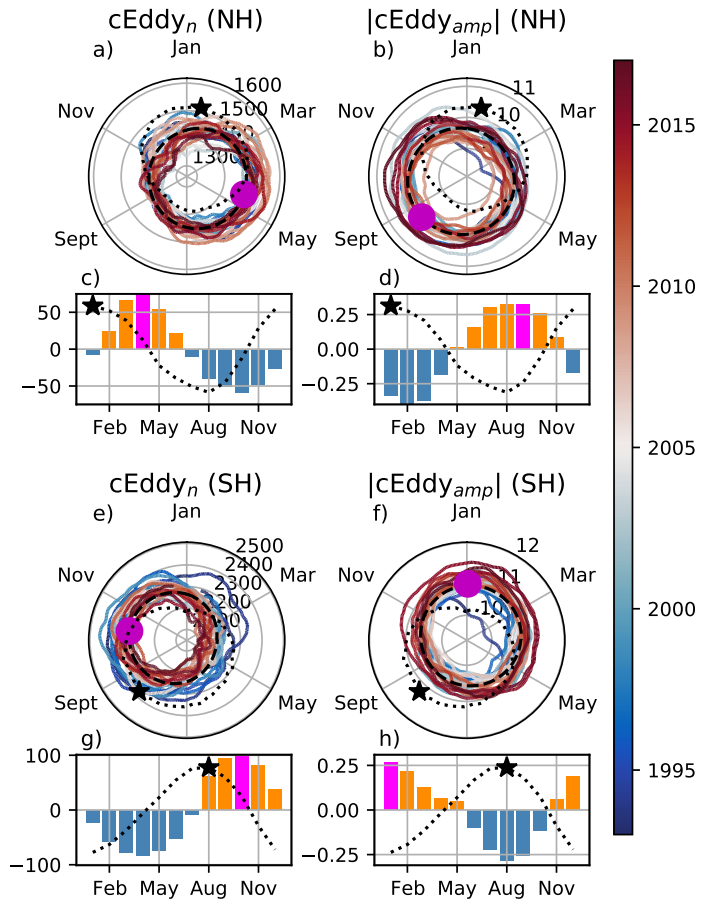
- a

**5 Trends****Figure 13**

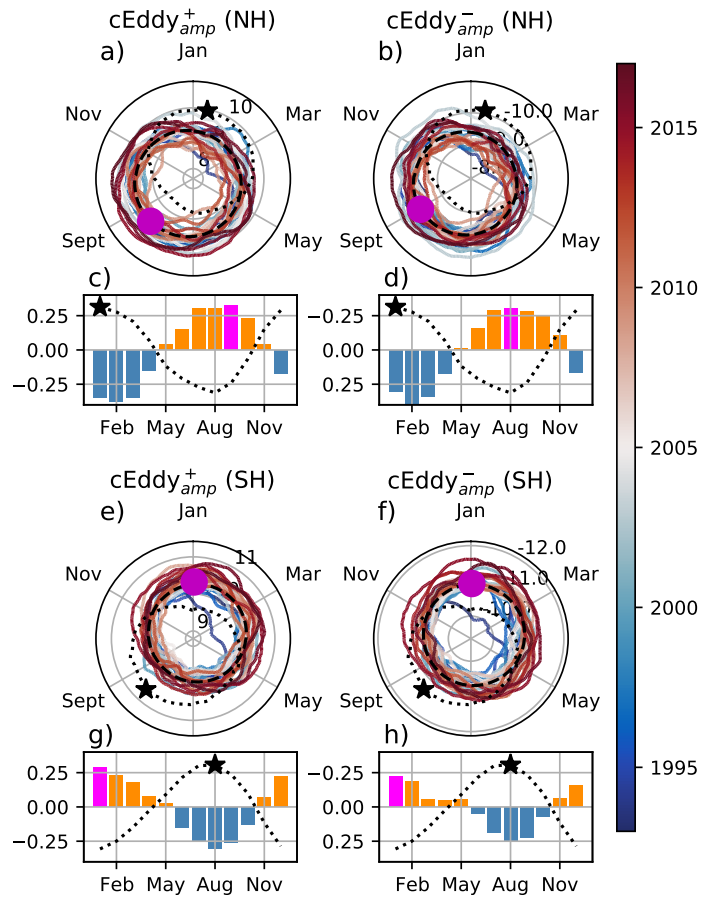
- The number and amplitude of coherent eddies from two eddy tracking algorithms show consistent trend patterns.
- In particular, we observe a decrease in the number of eddies in the southern ocean, as well as sectors in the North Atlantic and North Pacific.
- Meanwhile the amplitude seems to be increasing in those same regions.
- Some of these regions have undergone a readjustment to stronger winds, thus the observed trends in the eddy amplitude suggests an intensification of the coherent eddy field to an increase in the forcing.
- This increase is consistent with Martínez-Moreno et al. (2021)

**6 Regional****6.1 Boundary Currents****Figure 10**

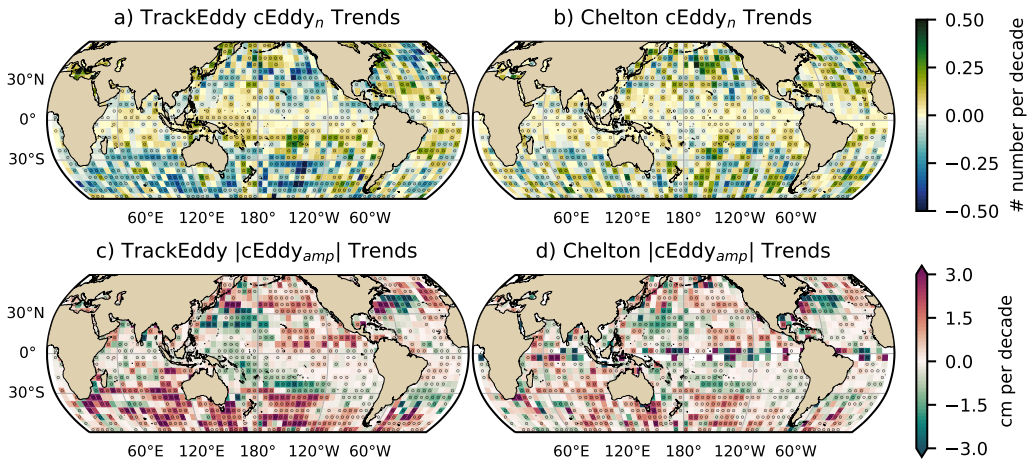
- Described similar to figure 7, 8, and 9
- Note that boundary currents have a consistent seasonal cycle in the positive and negative eddy amplitude.
- As expected, the seasonal cycle is opposite to BC in the northern hemisphere.



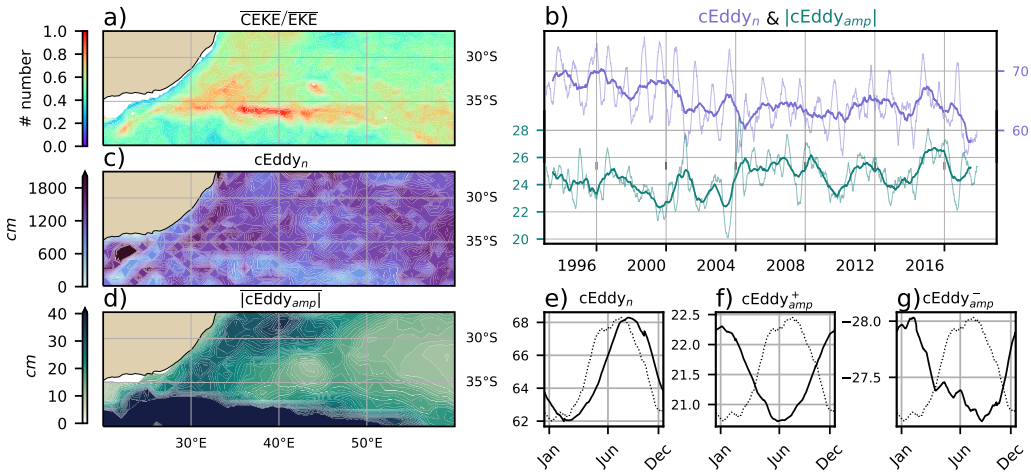
263 **Figure 6.** Hemispherical seasonality of the coherent eddy statistics; a,e) seasonal cycle of the  
 264 number of coherent eddies ( $cEddy_n$ ); b,f) seasonal cycle of the mean coherent eddy amplitude  
 265 ( $cEddy_{amp}$ ); c,g) seasonal cycle of the warm core coherent eddies amplitude (positive  $cEddy_{amp}$ );  
 266 d,h) seasonal cycle of the cold core coherent eddies amplitude (negative  $cEddy_{amp}$ ). Panels a,b  
 267 and c show the northern hemisphere seasonal cycle, while panels d,e, and f correspond to the  
 268 southern hemisphere. Dashed lines correspond to the seasonal cycle of the fields and dotted lines  
 269 show the seasonal cycle of the wind magnitude smoothed over 120 days (moving average). The  
 270 green and magenta stars show the maximum of the seasonal cycle for each field and the wind  
 271 magnitude, respectively. The line colors show the year.



274 **Figure 7.** Hemispherical seasonality of the coherent eddy statistics; a,e) seasonal cycle of the  
 275 number of coherent eddies ( $c\text{Eddy}_n$ ); b,f) seasonal cycle of the mean coherent eddy amplitude  
 276 ( $c\text{Eddy}_{amp}$ ); c,g) seasonal cycle of the warm core coherent eddies amplitude (positive  $c\text{Eddy}_{amp}^+$ );  
 277 d,h) seasonal cycle of the cold core coherent eddies amplitude (negative  $c\text{Eddy}_{amp}^-$ ). Panels a,b  
 278 and c show the northern hemisphere seasonal cycle, while panels d,e, and f correspond to the  
 279 southern hemisphere. Dashed lines correspond to the seasonal cycle of the fields and dotted lines  
 280 show the seasonal cycle of the wind magnitude smoothed over 120 days (moving average). The  
 281 green and magenta stars show the maximum of the seasonal cycle for each field and the wind  
 282 magnitude, respectively. The line colors show the year.



294 **Figure 8.** Trends of coherent eddy statistics. a) and b) Trends of the number of identified  
 295 coherent eddies from satellite observations identified using TrackEddy, and those reported in  
 296 Chelton's dataset. c) and e) Trends of the mean absolute value of identified coherent eddies am-  
 297 plitude from satellite observations identified using TrackEddy, and those reported in Chelton's  
 298 dataset. Gray stippling shows regions that are statistically significant above the 95% confidence  
 299 level.



307 **Figure 9.** Same as Figure 12 but for the Agulhas Current.

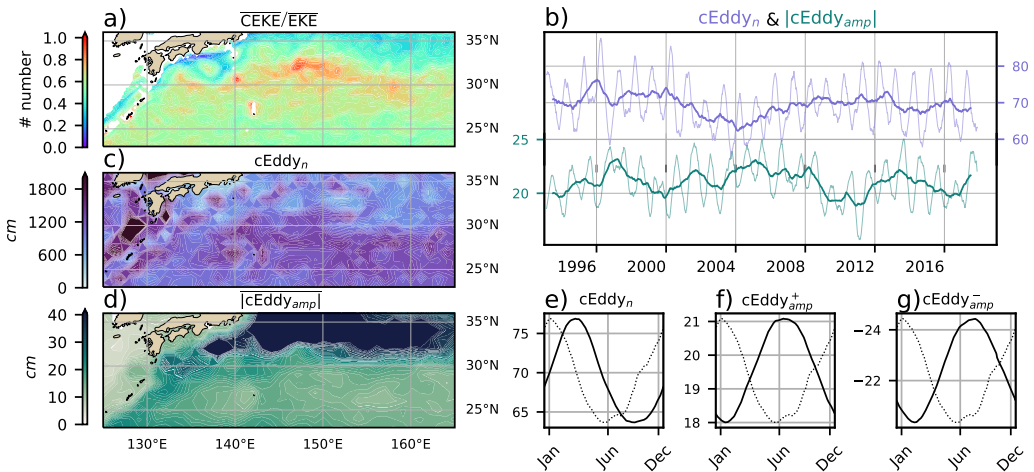


**Figure 10.** Same as Figure 12 but for the Kuroshio Current.

312

308

### Figure 11

309

310

311

- Described similar to figure 7, 8, and 9
- Note that boundary currents have a consistent seasonal cycle in the positive and negative eddy amplitude.

313

### Figure 12

314

315

316

317

- Described similar to figure 7, 8, and 9
- Note that boundary currents have a consistent seasonal cycle in the positive and negative eddy amplitude.
- Delete Fig 11 or 12, they are really similar. What do you think?

319

## 6.2 Eastern currents

320

### Figure 7

321

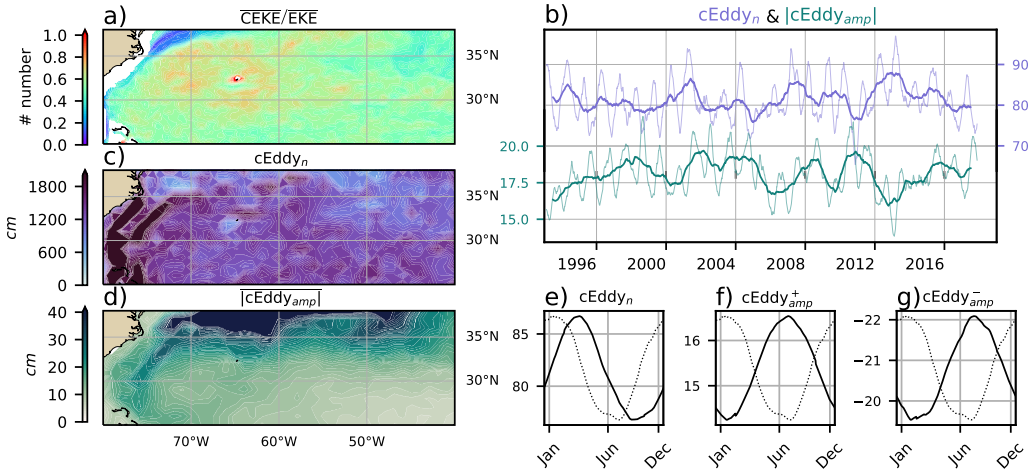
322

323

324

325

- South of the Leeuwin Current there is an important dominance fo the coherent eddy field, where it explains around 80% of the eddy kinetic energy.
- Although this region does not have a large EKE, we can observe a considerable amount of eddies across the region, but more importantly the coherent eddy amplitude is particularly large in those regions with coherent eddy dominance.

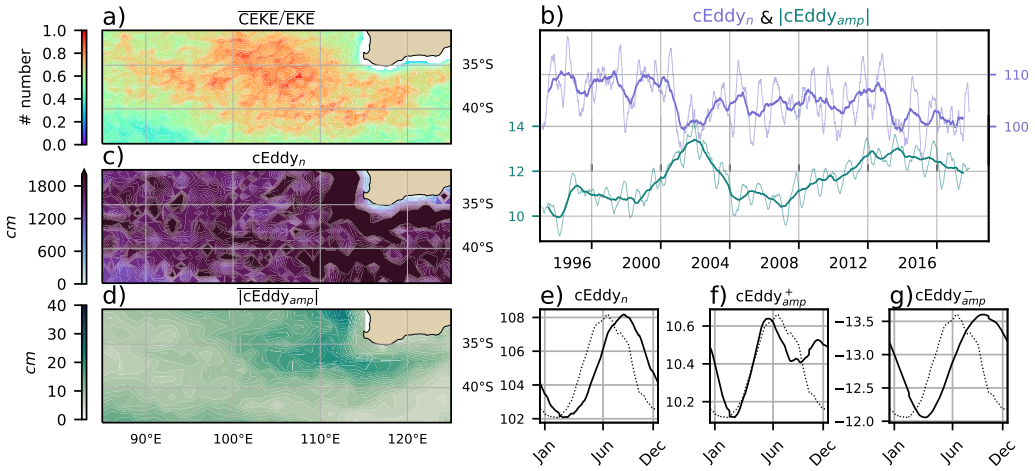


318 **Figure 11. Move to supplementary** Same as Figure 12 but for the Gulf Stream.

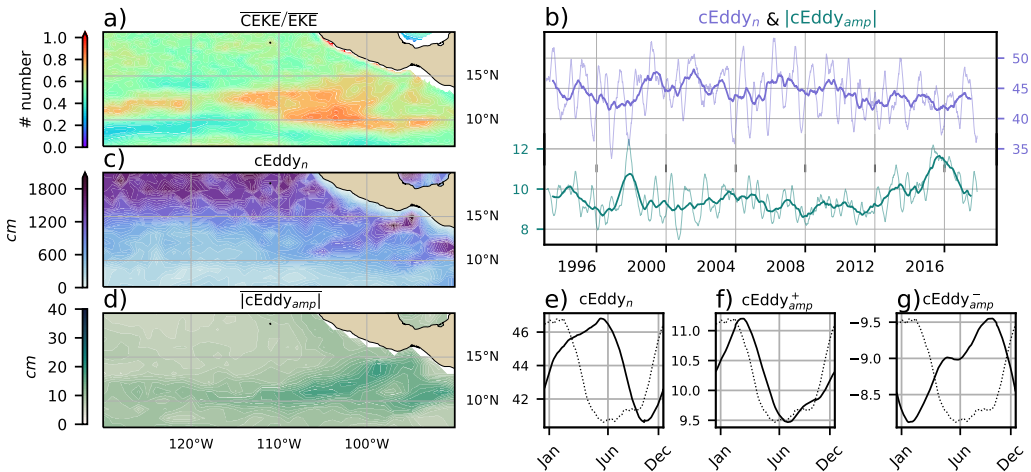
- 326 • The solid lines show an decrease in the number of eddies, but an increase in the  
327 eddy amplitude.  
328 • Moreover, the coherent eddy number peaks in August.  
329 • Meanwhile coherent eddies with the positive amplitude have a smaller amplitude  
330 than the negative, furthermore, the positive eddies peak in Jun and show a inter-  
331 annual modulation, while the negative eddies peak in October.  
332 • Research regional dynamics (Add here why we may expect this response.)

340 **Figure 9**

- 341 • Here we observe that the number of eddies and eddy amplitude are large in the  
342 area where the coherent eddies dominate the eddy field.  
343 • Dynamically, in this region eddies are generated due to Rossby wave propagation  
344 along the coast that becomes unstable and sheds eddies at the Tehuantepec Gulf.  
345 • The seasonal cycle shows a peak in Jun, while the positive amplitude is observed  
346 in March and the negative amplitude maximum occurs in September.  
347 • Research regional dynamics (Add here why we may expect this response.)



333 **Figure 12.** Climatology of the eddy field and coherent eddy field at the Leeuwin Current. a)  
 334 Ratio of mean coherent eddy kinetic energy ( $\overline{\text{CEKE}}$ ) versus mean eddy kinetic energy ( $\overline{\text{EKE}}$ ); b)  
 335 Thick lines show the running average over 2 years and thin lines show the running average over  
 336 90 days of the coherent eddy number sum and the average absolute coherent eddy amplitude; c)  
 337 Map of the number of eddies; d) Map of the average absolute coherent eddy amplitude; e) Sea-  
 338 sonal cycle of the number of eddies f) Seasonal cycle of the positive coherent eddy amplitude. g)  
 339 Seasonal cycle of the negative coherent eddy amplitude.



348 **Figure 13.** Same as Figure 12 but for the East Tropical Pacific.

349      **7 Summary and Conclusions**

350      **Acknowledgments**

351      Chelton & Schlax (2013) dataset was produced by SSALTO/DUACS and distributed by  
 352      AVISO+ (<https://www.aviso.altimetry.fr/>) with support from CNES, developed  
 353      and validated in collaboration with E.Mason at IMEDEA.

354      **References**

- 355      Arbic, B. K., Polzin, K. L., Scott, R. B., Richman, J. G., & Shriver, J. F. (2013).  
 356      On Eddy Viscosity, Energy Cascades, and the Horizontal Resolution of Gridded  
 357      Satellite Altimeter Products\*. *Journal of Physical Oceanography*, 43(2), 283–300.  
 358      doi: 10.1175/jpo-d-11-0240.1
- 359      Ashkezari, M. D., Hill, C. N., Follett, C. N., Forget, G., & Follows, M. J. (2016).  
 360      Oceanic eddy detection and lifetime forecast using machine learning methods.  
 361      *Geophysical Research Letters*, 43(23). doi: 10.1002/2016gl071269
- 362      Beron-Vera, F. J., Wang, Y., Olascoaga, M. J., Goni, G. J., & Haller, G. (2013). Ob-  
 363      jective Detection of Oceanic Eddies and the Agulhas Leakage. *Journal of Physical  
 364      Oceanography*, 43(7), 1426–1438. doi: 10.1175/JPO-D-12-0171.1
- 365      Bouali, M., Sato, O. T., & Polito, P. S. (2017). Temporal trends in sea surface tem-  
 366      perature gradients in the South Atlantic Ocean. *Remote Sensing of Environment*,  
 367      194, 100–114. doi: 10.1016/j.rse.2017.03.008
- 368      Callies, J., Flierl, G., Ferrari, R., & Fox-Kemper, B. (2015). The role of mixed-layer  
 369      instabilities in submesoscale turbulence. *Journal of Fluid Mechanics*, 788, 5–41.  
 370      doi: 10.1017/jfm.2015.700
- 371      Cane, M. A., Clement, A. C., Kaplan, A., Kushnir, Y., Pozdnyakov, D., Seager, R.,  
 372      ... Murtugudde, R. (1997). Twentieth-Century Sea Surface Temperature Trends.  
 373      *Science*, 275(5302), 957–960. doi: 10.1126/science.275.5302.957
- 374      Chelton, D. B., Gaube, P., Schlax, M. G., Early, J. J., & Samelson, R. M. (2011).  
 375      The influence of nonlinear mesoscale eddies on near-surface oceanic chlorophyll.  
 376      *Science*, 334(6054), 328–32. doi: 10.1126/science.1208897
- 377      Chelton, D. B., & Schlax, M. G. (2013). *Mesoscale eddies in altimeter observations  
 378      of ssh*.
- 379      Chelton, D. B., Schlax, M. G., Samelson, R. M., & de Szoeke, R. A. (2007). Global

- 380 observations of large oceanic eddies. *Geophysical Research Letters*, 34(15),  
381 L15606. doi: 10.1029/2007GL030812
- 382 CMEMS. (2017). The Ssalto/Duacs altimeter products were produced and dis-  
383 tributed by the Copernicus Marine and Environment Monitoring Service. *Aviso*  
384 *Dataset*. Retrieved from <https://www.aviso.altimetry.fr/>
- 385 Cui, W., Wang, W., Zhang, J., & Yang, J. (2020). Identification and census statis-  
386 tics of multicore eddies based on sea surface height data in global oceans. *Acta*  
387 *Oceanologica Sinica*, 39(1), 41–51. doi: 10.1007/s13131-019-1519-y
- 388 Faghmous, J. H., Frenger, I., Yao, Y., Warmka, R., Lindell, A., & Kumar, V. (2015,  
389 6). A daily global mesoscale ocean eddy dataset from satellite altimetry. *Scientific*  
390 *Data*, 2, 150028 EP -. doi: 10.1038/sdata.2015.28
- 391 Ferrari, R., & Wunsch, C. (2009). Ocean Circulation Kinetic Energy: Reservoirs,  
392 Sources, and Sinks. *Annual Review of Fluid Mechanics*, 41(1), 253–282. doi: 10  
393 .1146/annurev.fluid.40.111406.102139
- 394 Frenger, I., Gruber, N., Knutti, R., & Münnich, M. (2013). Imprint of Southern  
395 Ocean eddies on winds, clouds and rainfall. *Nature Geoscience*, 6(8), 608 EP -.  
396 doi: 10.1038/ngeo1863
- 397 Frenger, I., Münnich, M., Gruber, N., & Knutti, R. (2015). Southern Ocean eddy  
398 phenomenology. *Journal of Geophysical Research: Oceans*, 120(11), 7413-7449.  
399 doi: 10.1002/2015JC011047
- 400 Fu, L., Chelton, D., Le Traon, P., & Oceanography, M. R. (2010). Eddy dynamics  
401 from satellite altimetry. *Oceanography*, 23(4), 14-25. doi: 10.2307/24860859
- 402 Gill, A., Green, J., & Simmons, A. (1974). Energy partition in the large-scale ocean  
403 circulation and the production of mid-ocean eddies. *Deep Sea Res Oceanogr Abstr*,  
404 21(7), 499-528. doi: 10.1016/0011-7471(74)90010-2
- 405 Hogg, A. M., & Blundell, J. R. (2006). Interdecadal variability of the southern  
406 ocean. *Journal of Physical Oceanography*, 36(8), 1626-1645. doi: 10.1175/  
407 JPO2934.1
- 408 Hogg, A. M., Meredith, M. P., Chambers, D. P., Abrahamsen, E. P., Hughes,  
409 C. W., & Morrison, A. K. (2015). Recent trends in the Southern Ocean  
410 eddy field. *Journal of Geophysical Research: Oceans*, 120(1), 257-267. doi:  
411 10.1002/2014JC010470
- 412 Hu, S., Sprintall, J., Guan, C., McPhaden, M. J., Wang, F., Hu, D., & Cai,

- 413 W. (2020, 2). Deep-reaching acceleration of global mean ocean circulation  
414 over the past two decades. *Science Advances*, 6(6), eaax7727. doi:  
415 10.1126/sciadv.aax7727
- 416 Japan Meteorological Agency, Japan. (2013). *Jra-55: Japanese 55-year reanalysis,*  
417 *daily 3-hourly and 6-hourly data.* Boulder CO: Research Data Archive at the Na-  
418 tional Center for Atmospheric Research, Computational and Information Systems  
419 Laboratory. Retrieved from <https://doi.org/10.5065/D6HH6H41>
- 420 Kang, D., & Curchitser, E. N. (2017). On the Evaluation of Seasonal Variability of  
421 the Ocean Kinetic Energy. *Geophysical Research Letters*, 47, 1675-1583. doi: 10  
422 .1175/JPO-D-17-0063.1
- 423 Li, G., Cheng, L., Zhu, J., Trenberth, K. E., Mann, M. E., & Abraham, J. P. (2020).  
424 Increasing ocean stratification over the past half-century. *Nature Climate Change*,  
425 1–8. doi: 10.1038/s41558-020-00918-2
- 426 Martínez-Moreno, J., Hogg, A. M., England, M., Constantinou, N. C., Kiss, A. E.,  
427 & Morrison, A. K. (2021). Global changes in oceanic mesoscale currents over the  
428 satellite altimetry record. *Journal of Advances in Modeling Earth Systems*, 0(ja).  
429 doi: 10.1029/2019MS001769
- 430 Martínez-Moreno, J., Hogg, A. M., Kiss, A. E., Constantinou, N. C., & Morrison,  
431 A. K. (2019). Kinetic energy of eddy-like features from sea surface altime-  
432 try. *Journal of Advances in Modeling Earth Systems*, 11(10), 3090-3105. doi:  
433 10.1029/2019MS001769
- 434 Patel, R. S., Llort, J., Strutton, P. G., Phillips, H. E., Moreau, S., Pardo, P. C.,  
435 & Lenton, A. (2020). The Biogeochemical Structure of Southern Ocean  
436 Mesoscale Eddies. *Journal of Geophysical Research: Oceans*, 125(8). doi:  
437 10.1029/2020jc016115
- 438 Pilo, G. S., Mata, M. M., & Azevedo, J. L. L. (2015). Eddy surface properties and  
439 propagation at Southern Hemisphere western boundary current systems. *Ocean  
440 Science*, 11(4), 629–641. doi: 10.5194/os-11-629-2015
- 441 Qiu, B. (1999). Seasonal Eddy Field Modulation of the North Pacific Subtropical  
442 Countercurrent: TOPEX/Poseidon Observations and Theory. *Journal of Physical  
443 Oceanography*, 29(10), 2471–2486. doi: 10.1175/1520-0485(1999)029<2471:sefmot>2  
444 .0.co;2
- 445 Qiu, B., & Chen, S. (2004). Seasonal Modulations in the Eddy Field of the South

- 446 Pacific Ocean. *Journal of Physical Oceanography*, 34(7), 1515–1527. doi: 10.1175/  
447 1520-0485(2004)034<1515:smitef>2.0.co;2
- 448 Qiu, B., Chen, S., Klein, P., Sasaki, H., & Sasai, Y. (2014). Seasonal Mesoscale  
449 and Submesoscale Eddy Variability along the North Pacific Subtropical Coun-  
450 tercurrent. *Journal of Physical Oceanography*, 44(12), 3079–3098. doi:  
451 10.1175/JPO-D-14-0071.1
- 452 Ruela, R., Sousa, M. C., deCastro, M., & Dias, J. M. (2020). Global and regional  
453 evolution of sea surface temperature under climate change. *Global and Planetary  
454 Change*, 190, 103190. doi: 10.1016/j.gloplacha.2020.103190
- 455 Sasaki, H., Klein, P., Qiu, B., & Sasai, Y. (2014). Impact of oceanic-scale inter-  
456 actions on the seasonal modulation of ocean dynamics by the atmosphere. *Nature  
457 Communications*, 5(1), 5636. doi: 10.1038/ncomms6636
- 458 Schubert, R., Schwarzkopf, F. U., Baschek, B., & Biastoch, A. (2019). Submesoscale  
459 Impacts on Mesoscale Agulhas Dynamics. *Journal of Advances in Modeling Earth  
460 Systems*, 11(8), 2745–2767. doi: 10.1029/2019ms001724
- 461 Siegel, D., Peterson, P., DJ, M., Maritorena, S., & Nelson, N. (2011). Bio-optical  
462 footprints created by mesoscale eddies in the Sargasso Sea. *Geophysical Research  
463 Letters*, 38(13), n/a-n/a. doi: 10.1029/2011GL047660
- 464 Uchida, T., Abernathey, R., & Smith, S. (2017). Seasonality of eddy kinetic energy  
465 in an eddy permitting global climate model. *Ocean Modelling*, 118, 41–58. doi: 10  
466 .1016/j.ocemod.2017.08.006
- 467 Wunsch, C. (2020). Is The Ocean Speeding Up? Ocean Surface Energy Trends.  
468 *Journal of Physical Oceanography*, 50(11), 1–45. doi: 10.1175/jpo-d-20-0082.1
- 469 Wunsch, C., & Ferrari, R. (2004). VERTICAL MIXING, ENERGY, AND THE  
470 GENERAL CIRCULATION OF THE OCEANS. *Annual Review of Fluid Me-  
471 chanics*, 36(1), 281–314. doi: 10.1146/annurev.fluid.36.050802.122121
- 472 Wyrtki, K., Magaard, L., & Hager, J. (1976). Eddy energy in the oceans. *Journal of  
473 Geophysical Research*, 81(15), 2641-2646. doi: 10.1029/JC081i015p02641
- 474 Yue, S., & Wang, C. (2004). The Mann-Kendall Test Modified by Effective Sample  
475 Size to Detect Trend in Serially Correlated Hydrological Series. *Water Resources  
476 Management*, 18(3), 201–218. doi: 10.1023/b:warm.0000043140.61082.60